Contents lists available at ScienceDirect

Digital Chinese Medicine

journal homepage: http://www.keaipublishing.com/dcmed

Multi-target inhibition property of *Persicaria hydropiper* phytochemicals against gram-positive and gram-negative bacteria via molecular docking, dynamics simulation, and ADMET analysis

Golak Majumdar, Shyamapada Mandal*

Department of Zoology, University of Gour Banga, Malda, West Bengal 732103, India

ARTICLE INFO

Article history
Received 01 October 2024
Accepted 27 December 2024
Available online 25 March 2025

Keywords
Persicaria hydropiper phytochemicals
Molecular docking
Molecular dynamics simulation
Bacterial pathogenicity-related proteins
Pharmacokinetics

ABSTRACT

Objective To evaluate the antibacterial potential of bioactive compounds from *Persicaria hydropiper* (L.) (*P. hydropiper*) against bacterial virulence proteins through molecular docking (MD) and experimental validation.

Methods Six bioactive compounds from *P. hydropiper* were investigated: catechin (CAT1), hyperin (HYP1), ombuin (OMB1), pinosylvin (PSV1), quercetin 3-sulfate (QSF1), and scutellarein (SCR1). Their binding affinities and potential binding pockets were assessed through MD against four bacterial target proteins with Protein Data Bank identifiers (PDB IDs): topoisomerase IV from *Escherichia coli* (*E. coli*) (PDB ID: 3FV5), *Staphylococcus aureus* (*S. aureus*) gyrase ATPase binding domain (PDB ID: 3U2K), CviR from *Chromobacterium violaceum* (*C. violaceum*) (PDB ID: 3QP1), and glycosyl hydrolase from *Pseudomonas aeruginosa* (*P. aeruginosa*) (PDB ID: 5BX9). Molecular dynamics simulations (MDS) were performed on the most promising compound-protein complexes for 50 nanoseconds (ns). Drug-likeness was evaluated using Lipinski's Rule of Five (RO5), followed by absorption, distribution, metabolism, excretion, and toxicity (ADMET) analysis using SwissADME and pkCSM web servers. Antibacterial activity was evaluated through disc diffusion assays, testing both individual compounds and combinations with conventional antibiotics [cefotaxime (CTX1, 30 μg/disc), ceftazidime (CAZ1, 30 μg/disc), and piperacillin (PIP1, 100 μg/disc)].

Results MD revealed strong binding affinity (ranging from – 9.3 to – 5.9 kcal/mol) for all compounds, with CAT1 showing exceptional binding to 3QP1 (– 9.3 kcal/mol) and 5BX9 (– 8.4 kcal/mol). MDS confirmed the stability of CAT1-protein complexes with binding free energies of – 84.71 kJ/mol (5BX9-CAT1) and – 95.59 kJ/mol (3QP1-CAT1). Five compounds (CAT1, SCR1, PSV1, OMB1, and QSF1) complied with Lipinski's RO5 and showed favorable ADMET profiles. All compounds were non-carcinogenic, with CAT1 classified in the lowest toxicity class (VI). In antibacterial assays, CAT1 demonstrated significant activity against both gram-positive bacteria [*Streptococcus pneumoniae* (*S. pneumoniae*), *S. aureus*, and *Bacillus cereus* (*B. cereus*)] [zone diameter of inhibition (ZDI): 10 – 22 mm] and gram-negative bacteria [*Acinetobacter baumannii* (*A. baumannii*), *E. coli*, and *P. aeruginosa*] (ZDI: 14 – 27 mm). Synergistic effects were observed when CAT1 was combined with antibiotics and the growth inhibitory indices (GII) was 0.69 – 1.00.

*Corresponding author: Shyamapada Mandal, E-mail: sam.micro11@ugb.ac.in.

Peer review under the responsibility of Hunan University of Chinese Medicine.

DOI: 10.1016/j.dcmed.2025.03.007

Citation: MAJUMDAR G, MANDAL S. Multi-target inhibition property of *Persicaria hydropiper* phytochemicals against gram-positive and gram-negative bacteria via molecular docking, dynamics simulation, and ADMET analysis. Digital Chinese Medicine, 2025, 8(1): 76-89.

Conclusion *P. hydropiper* bioactive compounds, particularly CAT1, show promising antibacterial potential through multiple mechanisms, including direct inhibition of bacterial virulence proteins and synergistic activity with conventional antibiotics. The favorable pharmacological properties and low toxicity profiles support their potential development as therapeutic agents against bacterial infections.

1 Introduction

Bacterial resistance to conventional antibiotics poses a major challenge in combating infections caused by both gram-positive and gram-negative bacteria [1]. Both nosocomial and community-acquired infections contribute to a large number of deaths worldwide [2]. In 2019, there were 1.27 million deaths associated with bacterial antimicrobial resistance (AMR) and currently each year 4.95 million deaths occur due to bacterial AMR, including *Escherichia coli* (*E. coli*) and *Klebsiella pneumoniae* (*K. pneumoniae*) resisting third-generation cephalosporins, *K. pneumoniae* and *Acinetobacter baumannii* (*A. baumannii*) exhibiting carbapenem resistance, *E. coli* showing fluoroquinolone resistance, *Staphylococcus aureus* (*S. aureus*) with methicillin resistance, as well as *Streptococcus pneumoniae* (*S. pneumoniae*) and *Pseudomonas aeruginosa* (*P. aeruginosa*) showing multidrug resistance [1-3]. The World Health Organization (WHO) has indicated that a dozen families of bacteria have been recognized as being antibiotic-resistant and have been designated as priority pathogens, which are further subdivided into three categories: critical, high, and medium [4]. Similarly, nosocomial infection caused by the *Enterococcus faecium*, *S. aureus*, *K. pneumoniae*, *A. baumannii*, *P. aeruginosa*, and *Enterobacter* species (ESKAPE) pathogens have developed resistance to multiple antibiotics of different classes [5]. With bacteria continually evolving multidrug resistance mechanisms that undermine the effectiveness of antibiotics, alternative treatment options are urgently needed, considering the lack of effective therapies free of significant toxicity risks [4]. The rapidly growing crisis of antibiotic resistance must be addressed by identifying phytochemicals with antibacterial activity. Although some natural alternatives including bacteriocins, probiotics, honey, vaccines, phytochemicals, and antimicrobial peptides are available, it's still crucial to carry out further exploration into the employment of phytochemicals for suppressing bacterial quorum sensing and biofilm formation [6, 7]. Throughout the history of humanity, medicinal plants have served as a crucial means to treat diseases, especially in regions such as China, India, among other countries [8]. Traditional medicinal systems have survived and thrived in modern times due to their considerable potential in disease treatment and minimal side effects [8].

Persicaria hydropiper (L.) (*P. hydropiper*) is a popular traditionally important medicinal plant with powerful and potent antibacterial activity [9]. The plant contains various phytochemicals that can address a range of ailments, including pain, kidney stones, abdominal issues, hemorrhoids, ulcers, jaundice, and it has anthelmintic properties [9]. In traditional Chinese medicine (TCM), *P. hydropiper* has served as a condiment. The crushed leaves of the plant are used for treating a variety of skin problems, like scabies, ringworms, boils, abscesses, ulcers, and carbuncles. The extracts derived from the plant are also applied to treat bites from dogs, snakes, and insects due to its safe and non-toxic properties [9]. Despite its widespread use in TCM, the studies conducted on *P. hydropiper*-derived phytochemicals regarding their therapeutic potential and pharmacological properties remain limited. Therefore, the bioactive compounds from *P. hydropiper* hold significant promise for future drug development [8]. Furthermore, bacterial enzymes, which are crucial for bacterial growth, survival, and pathogenicity, have emerged as key targets in the pursuit of cost-effective small-molecule drug discovery. Computational methods, such as molecular docking (MD), provide an important approach for identifying these drugs [10]. MD can predict the binding affinity between small molecule drugs (ligands) and target proteins in drug discovery, thereby revealing potential interaction modes that play a key role in the formation of stable complexes [11]. In medicinal chemistry, molecular dynamics simulations (MDS) of protein-ligand complexes can examine specific events and properties within the time scale from nanoseconds to microseconds at the atomic level, contributing to the understanding of their structural dynamics and features [10, 11]. Meanwhile, absorption, distribution, metabolism, excretion, and toxicity (ADMET) analysis evaluates the drug-likeness, safety, and efficacy of lead small molecules [12]. Among the reported bacterial target proteins, topoisomerase IV (3FV5), DNA gyrase ATPase binding domain (3U2K), CviR LuxR (3QP1), and glycosyl hydrolase (5BX9) are vital for the metabolic activities and survival of both gram-positive and gram-negative bacteria [13, 14]. Therefore, this study aimed to evaluate the binding affinity and stability between *P. hydropiper* phytochemicals and bacterial virulence proteins through molecular docking and molecular dynamics simulations, assess the drug-likeness of these compounds through ADMET profiling, and investigate the antibacterial efficacy of catechin, both alone and in combination with conventional antibiotics, through experimental validation.

2 Data and methods

2.1 Retrieval and preparation of phytochemical ligands

In this study, six phytochemicals from *P. hydropiper* were selected: catechin (PubChem CID: 9064, CAT1), hyperin (PubChem CID: 5281643, HYP1), ombuin (PubChem CID: 5320287, OMB1), pinosylvin (PubChem CID: 5280457, PSV1), quercetin 3-sulfate (PubChem CID: 5280362, QSF1), and scutellarein (PubChem CID: 5281697, SCR1). Additionally, two broad-spectrum antibiotics were included as reference compounds: cefotaxime (PubChem CID: 5742673, CTX1) and ciprofloxacin (PubChem CID: 2764, CIP1). All compounds were retrieved from PubChem database (https://pubchem.ncbi.nlm.nih.gov/) [8]. The ligand structures were prepared using University of California, San Francisco (UCSF) Chimera (https://www.cgl.ucsf.edu/chimera/download.html) [15]. The preparation process included adding hydrogen atoms and applying Gasteiger charges to optimize the structures for MD studies.

2.2 Retrieval and preparation of bacterial target protein

Four pathogenic bacterial proteins were selected for this study: topoisomerase IV from *E. coli* [Protein Data Bank identifier (PDB ID): 3FV5], *S. aureus* gyrase ATPase binding domain (PDB ID: 3U2K), CviR from *Chromobacterium violaceum* (*C. violaceum*) (PDB ID: 3QP1), and glycosyl hydrolase from *P. aeruginosa* (PDB ID: 5BX9). Their three-dimensional (3D) crystal structures were downloaded from the Research Collaboratory for Structural Bioinformatics (RCSB) Protein Data Bank and prepared using UCSF Chimera by removing co-crystallized ligands, solvents, and ions, adding Gasteiger charges and hydrogen atoms, and saving them in PDB format. Binding pockets were identified using F-pocket 1.0 (https://mobyle2.rpbs.univ-paris-diderot.fr/cgi-bin/portal.py#forms::fpocket), and Ψ/Φ bond analysis, including torsion and backbone conformations, was assessed with Ramachandran plots using the Protein Geometry and Structure Validation (PROCHECK) server (https://saves.mbi.ucla.edu/). The Ramachandran plot indicated that were four protein structures were acceptable for MD and MDS, with more than 90% of residues positioned in the most favored regions at a resolution of 2.0 Ångström (Å).

2.3 MD analysis and binding site identification

MD is a key tool in structural molecular biology and computer-assisted drug design [15]. MD aims to generate a protein ligand complex with optimized conformations, which is intended to possess less binding energy (BE) [15, 16]. MD was performed for all six phytochemicals and two antibiotics against the four target proteins using UCSF Chimera inbuilt AutoDock Vina and CB-Dock2 web server (https://cadd.labshare.cn/cb-dock2/index.php). Grid boxes were defined around the active sites of each protein with the following dimensions and coordinates: 3FV5 (41 × 44 × 42 Å^3, X = 19, Y = 0.6, Z = 6), 3QP1 (45 × 45 × 45 Å^3, X = 17, Y = 17, Z = 45), 3U2K (45 × 45 × 45 Å^3, X = 6, Y = 9, Z = 22), and 5BX9 (70 × 70 × 70 Å^3, X = 6, Y = 35, Z = – 10). The BE cut-off values ⩽ – 6.5 kcal/mol were considered significant for docking affinity analysis [15, 16]. Protein binding sites were analyzed using the CAVER web server v1.2 (https://loschmidt.chemi.muni.cz/caverweb/). This analysis identified tunnels and catalytic pockets based on quantitative parameters, including relevance scores, cavity volume, and druggability indices. The protein-ligand interactions were further evaluated using CaverDock to assess the binding modes through an induced-fit mechanism [17].

2.4 Pharmacological property analysis

The pharmacological properties of selected ligands were evaluated through ADMET predictions using Swiss ADME (http://www.swissadme.ch/) and pkCSM (http://biosig.unimelb.edu.au/pkcsm/prediction). Bioavailability radar and ADMET analysis were used to assess the drug-likeness of the compounds [18]. Drug-likeness prediction was based on Lipinski's Rule of Five (RO5), which includes four key parameters: no more than 5 hydrogen bond donors, no more than 10 hydrogen bond acceptors, molecular mass less than 500 Da, and octanol-water partition coefficient (log P) not greater than 5 [18]. Oral bioavailability was assessed using the bioavailability radar provided by SwissADME. Six physicochemical parameters were analyzed: lipophilicity, estimated using XLOGP3 (log P values between – 0.7 and 5.0); molecular weight (150 – 500 g/mol); topological polar surface area (TPSA) (20 – 130 Å^2); aqueous solubility, predicted using the ESOL model (log S values between – 6 and 0); saturation, measured as the fraction of sp^3 carbons (0.25 – 1.00); and molecular flexibility, assessed by the number of rotatable bonds (0 – 9) [19]. The Brain Or IntestinaL EstimateD permeability (BOILED-Egg) model was employed to evaluate passive gastrointestinal absorption and blood-brain barrier (BBB) permeability using SwissADME. This model provides predictions based on the compounds' lipophilicity and polar surface area [19-21].

2.5 Carcinogenicity prediction

Carcinogenicity predictions for the bioactive compounds were performed using the CarcinoPred-EL web server (http://112.126.70.33/toxicity/CarcinoPred-EL/). The simplified molecular-input line-entry system (SMILES) notation of each compound was used as input for the analysis. The web server employs three advanced ensemble learning models: extreme gradient boosting (XGBoost), random forest (RF), and support vector machine (SVM). These

models were used to predict the carcinogenicity of the compounds containing more than three carbon atoms. Based on the analysis, the compounds were categorized as carcinogen (average probability value greater than 0.5) and non-carcinogens (average probability value less than 0.5) [22].

2.6 Toxicity class and median lethal dose (LD_{50}) value determination

The toxicity class and LD_{50} value of bioactive compounds were assessed using the ProTox II web server v3.0 (https://tox.charite.de/protox3/). The toxicity classification in the web server followed the guidelines of the Globally Harmonized System (GHS) [23]. Based on the LD_{50} values, compounds were categorized into six toxicity classes: class I: fatal if swallowed ($LD_{50} \leqslant 5$ mg/kg), class II: fatal if swallowed (5 mg/kg < $LD_{50} \leqslant 50$ mg/kg), class III: toxic if swallowed (50 mg/kg < $LD_{50} \leqslant 300$ mg/kg), class IV: harmful if swallowed (300 mg/kg < $LD_{50} \leqslant 2\,000$ mg/kg), class V: may be harmful if swallowed (2 000 mg/kg < $LD_{50} \leqslant 5\,000$ mg/kg), and class VI: non-toxic (LD_{50} > 5 000 mg/kg) [24].

2.7 MDS and stability analysis

Based on MD results and the established BE threshold ($\leqslant$ – 6.5 kcal/mol) from previous study [15], CAT1 exhibited the strongest binding affinity and was selected for MDS. The simulations were performed with two bacterial proteins, 3QP1 and 5BX9, which showed the most favorable interactions with CAT1. The study aimed to evaluate the stability and dynamics of the protein-ligand complexes. Simulations were conducted for 50 nanoseconds (ns) using GROMACS 2021 (www.gromacs.org) with topology files prepared via CHARMM General Force Field (CGenFF) [23]. Complex systems were neutralized with water and ions, followed by energy minimization to prevent steric clashes. A two-step equilibration process included a 10 ns NVT (constant number of particles, volume, and temperature) simulation using the V-rescale thermostat and Particle Mesh Ewald for electrostatics, followed by a 50 ns NPT (constant number of particles, pressure, and temperature) simulation at 300 K and 1 bar pressure. Position restraints were then released, and the production phase was performed for an additional 10 ns. Stability metrics such as root-mean-square deviation (RMSD), root-mean-square fluctuation (RMSF), radius of gyration, and TPSA were analyzed. Free binding energy of the protein-ligand complexes was calculated using linear interaction energy as described previously [24-26].

2.8 Experimental validation of CAT1 antibacterial activity

The antibacterial activity of CAT1 (97% purity) and antibiotic discs [piperacillin (PIP1) (100 μg/disc), ceftazidime (CAZ1) (30 μg/disc), and cefotaxime (CTX1) (30 μg/disc)] were sourced from Tokyo Chemical Industry (TCI), India and Hi-Media, India, respectively. CAT1 stock solution was prepared in sterile distilled water at a concentration of 1 000 μg/mL. Four working concentrations (125, 250, 375, and 500 μg/mL) were prepared through serial dilution for antibacterial activity testing. The antibacterial activity was evaluated using the disc diffusion method on nutrient agar plates (Hi-Media, India). Sterile discs of 6 mm diameter were impregnated with different concentrations of CAT1. Sterile disc was used for the disc diffusion method on nutrient agar plates to test antibacterial activity against six pathogenic bacterial strains, including gram-positive (*S. pneumoniae*, *S. aureus*, and *B. cereus*) and gram-negative (*A. baumannii*, *E. coli*, and *P. aeruginosa*). Antibiotic susceptibility testing for each bacterial strain was also performed using nutrient agar plates [27].

2.9 Combined antibacterial activity of CAT1 and antibiotics

The combined antibacterial activity was evaluated using CAT1 (250 μg/disc) in combination with three antibiotics against the six pathogenic bacterial strains, including three gram-positive (*S. pneumoniae*, *S. aureus*, and *B. cereus*) and three gram-negative (*P. aeruginosa*, *A. baumannii*, and *E. coli*) bacteria. The zone diameter of inhibition (ZDI) was measured for each combination to determine its combined efficacy. The growth inhibitory index (GII) was calculated using the following formula: GII = ZDI in combination/[total of ZDIs of two agents in a single action (antibiotic and CAT1)]. The interpretation of GII values was as follows: values less than 0.5 indicated antagonistic activity, values greater than 0.5 indicated synergistic activity, and values equal to 0.5 indicated additive activity [28].

2.10 Statistical analysis

Data analysis was conducted using Microsoft Excel 2013 (v15.0.4454.1503). Descriptive statistics, including mean, percentages, and ranges, were calculated to summarize the bacterial growth inhibition indices. Bar charts were created in Excel to visualize the antibacterial activity. Additionally, MDS graphs were generated using the Linux-based XMGRACE software (v5.1.22).

3 Results

3.1 MD of bioactive compounds from *P. hydropiper*

Four bacterial proteins were docked with six phytochemical ligands and two antibiotics, and their interactions were analyzed (Supplementary Table S1 and S2). The BE ranged from – 5.9 to – 9.3 kcal/mol, while with antibiotics,

BE ranged from – 6.1 to – 7.2 kcal/mol (Supplementary Figure S1 and S2). The phytochemical ligands, complexed with *E. coli* 3FV5, exhibited BE ranging from – 5.9 to – 7.1 kcal/mol (Supplementary Table S1). Topoisomerase IV with OMB1 gave the lowest BE of – 7.1 kcal/mol through formation of two conventional hydrogen bonds. The bonds involved amino acid residues Arg132 and Glu46, with bond lengths of 2.69 Å and 2.39 Å, respectively. CAT1, SCR1, QSF1, PSV1, and HYP1 showed similar types of bonds (Supplementary Table S1 and Figure 1).

The *S. aureus* 3U2K displayed binding energies with all six ligands, ranging from – 6.5 to – 8.4 kcal/mol (Supplementary Table S1). The lowest BE was observed with OMB1 (– 8.4 kcal/mol), which formed four conventional hydrogen bonds with Arg84 (2.77 Å), Thr173 (2.41 Å), Glu58 (2.59 Å), and Asp81 (2.20 Å). The interaction modes of remaining ligands were represented (Supplementary Table S1 and Figure S1). The binding affinities of all six ligands with 3QP1 ranged from – 6.5 to – 9.3 kcal/mol (Supplementary Table S1). The highest negative BE was recorded with CAT1 at – 9.3 kcal/mol. The CviR 3QP1 protein interacted with CAT1 through two conventional hydrogen bonds involving Ser155 (2.14 Å) and Asp97 (3.50 Å). Similar type of hydrogen and hydrophobic interaction of the five bioactive compounds were shown in Supplementary Table S1 and Figure S2.

5BX9 from *P. aeruginosa* displayed BE ranging from – 8.2 to – 8.4 kcal/mol for all the ligands (Supplementary Table S1). The lowest BE was observed with PSV1, which formed one conventional hydrogen bond with Gln241 (2.96 Å) (Supplementary Table S1 and Figure S3). To compare the docking results, besides the inbuilt AutoDock Vina in UCSF Chimera, the CB-Dock2 web tool was also applied [17]. The BE of 3FV5 with CAT1, SCR1, QSF1, PSV1, OMB1, HYP1, CTX1, and CIP1 were – 6.6, – 7.0, – 6.4, – 5.9, – 6.7, – 6.3, – 6.5, and – 5.8 kcal/mol, respectively. For 3U2K, these ligands exhibited BE ranging from – 7.5 to – 6.4 kcal/mol. Docking with 3QP1 showed BE ranging from – 9.0 to – 6.1 kcal/mol, while for 5BX9, values ranged from – 9.4 to – 7.2 kcal/mol (Supplementary Table S2). Four bacterial protein channels were identified, with a relevance score of 100 for all receptor molecules. The volume of the catalytic sites ranged from 416 to 1 524 Å^3, while the druggability scores of the catalytic sites fluctuated between 0.54 and 0.92. Additionally, the top ligand CAT1 exhibited CaverDock scores ranging from – 1.8 to – 6.5 kcal/mol (Supplementary Table S3) [17]. Both MD tools showed similar results with interaction energies consistently lower than – 6.5 kcal/mol, indicating strong binding affinity toward the bacterial target proteins [15, 16].

3.2 Pharmacological properties of phytochemicals

Table 1 depicts Lipinski's RO5 properties based on the ligand's pharmacophore characteristics of the ligands. Molecular weights ranging from 212.24 to 464.38, log *P* values ranging from – 0.538 9 to 3.268 2, H-bond acceptors ranging from 6 to 12, and H-bond donors ranging from 2 to 8. All the ligand molecules except hyperin (two

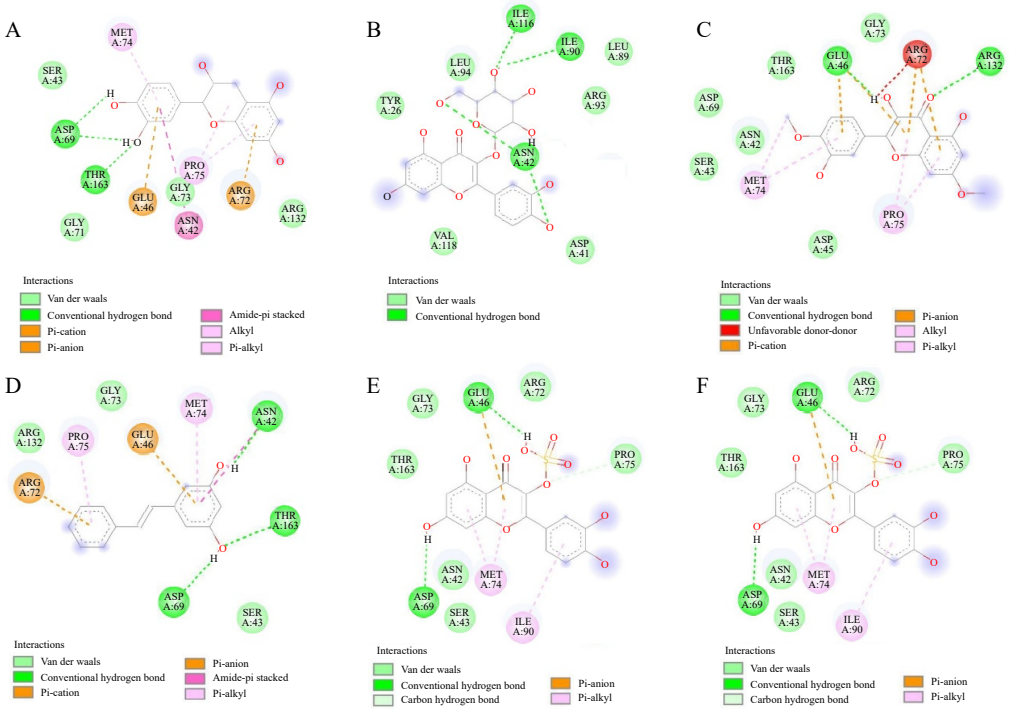

Figure 1 Two dimensional (2D) interaction of docked complex of 3FV5 with six phytochemicals from *P. hydropiper* A, CAT1. B, HYP1. C, OMB1. D, PSV1. E, QSF1. F, SCR1.

violations) obeyed Lipinski's RO5 with zero violations, indicating drug-like properties. Oral bioavailability was assessed with SwissADME and pkCSM (Table 2 and Supplementary Figure S4). A total of six ligand molecules were screened for ADMET properties (Table 3).

The ADMET properties of these six bioactive compounds were thoroughly investigated. Three absorption parameters were analyzed: water solubility (ranging from – 3.53 to – 2.94 mol/L), Caco-2 permeability (ranging from – 0.639 to 1.371), and intestinal absorption (ranging from 34.39% to 90.86%). Regarding distribution, the fraction unbound ranged from 0.087 to 0.161, BBB permeability ranged from – 1.812 to 0.112, and central nervous system permeability ranged from – 5.075 to – 1.744. Five metabolism parameters underwent evaluation. Among them, none of the compounds served as substrates of CYP2D6,

Table 1 Lipinski's RO5 for six phytochemicals from *P. hydropiper*

Phytochemical	Molecular weight (g/mol)	Log *P*	H-bond acceptor	H-bond donor	Lipinski's RO5 violation
CAT1	290.00	1.540 0	6	5	0
QSF1	382.30	1.464 0	10	5	0
SCR1	286.24	2.282 4	6	4	0
PSV1	212.24	3.268 2	2	2	0
OMB1	330.29	2.594 0	7	3	0
HYP1	464.38	– 0.538 9	12	8	2

Table 2 Bioavailability radar of selected phytochemicals from *P. hydropiper*

Phytochemical	Lipophilicity	Size	Solubility	Polarity	Flexibility	Saturation	Bioavailability score
CAT1	0.36	290.00	– 2.24	110.38	3	0	0.55
QSF1	1.79	382.30	– 5.25	183.11	3	0	0.11
SCR1	2.66	286.24	– 3.82	111.13	1	0	0.55
PSV1	3.48	212.24	– 4.01	40.46	2	0	0.55
OMB1	3.28	330.29	– 5.25	109.36	3	0.12	0.55
HYP1	0.36	464.38	– 1.51	210.51	4	0.29	0.17

Table 3 ADMET properties of selected phytochemicals from *P. hydropiper*

Parameter	Absorption			Distribution			Metabolism			
	Water solubility (mol/L)	Caco-2 permeability (log papp in 10^{-6} cm/s)	Intestinal absorption (human)	Fraction unbound (human)	BBB permeability (log BB)	CNS permeability (log PS)	CYP2D6 substrate	CYP3A4 substrate	CYP1A2 inhibitor	CYP2C19 inhibitor
Catechin	– 3.14	– 0.349	73.17	0.158	– 1.094	– 3.306	No	No	No	No
Quercetin 3-sulfate	– 2.94	– 0.639	34.39	0.158	– 1.697	– 4.189	No	No	No	No
Scutellarein	– 3.06	– 0.004	69.89	0.121	– 1.276	– 2.473	No	No	Yes	No
Pinosylvin	– 3.53	1.632	90.86	0.087	0.112	– 1.744	No	Yes	Yes	Yes
Ombuin	– 3.39	1.371	84.13	0.161	– 1.331	– 3.297	No	No	Yes	No
Hyperin	– 3.09	– 0.091	39.38	0.143	– 1.812	– 5.075	No	No	No	No

Parameter	Metabolism	Excretion		Toxicty						
	CYP2C9 inhibitor	Total clearance [mL/(min·kg)]	Renal OCT2 substrate	AMES toxicity	Max tolerated dose (human) [mg/(kg·d)]	Oral rat acute toxicity (LD50) (mol/kg)	Hepatotoxicity	Saturation (Fraction Csp3)	Bioavailability score	Synthetic accessibility
Catechin	No	0.270	No	Yes	0.545	2.074	No	0.20	0.55	3.50
Quercetin 3-sulfate	No	0.792	No	Yes	0.719	2.278	Yes	0.00	0.11	3.54
Scutellarein	No	0.511	No	No	0.781	2.347	No	0.00	0.55	3.04
Pinosylvin	Yes	0.167	No	No	0.761	1.923	No	0.00	0.55	1.98
Ombuin	No	0.766	No	Yes	0.763	2.341	No	0.12	0.55	3.41
Hyperin	No	0.738	No	Yes	0.934	2.771	No	0.29	0.17	5.32

while PSV1 was a substrate of CYP3A4. Additionally, none of the compounds inhibited CYP2C19 or CYP2D6, except for PSV1. However, CAT1, QSF1, and HYP1 were the three inhibitors of CYP1A2. For excretion, two parameters were considered: none of the compounds served as substrates of the renal OCT transporter, and the total clearance ranged from 0.167 to 0.792 mL/(min·kg). The maximum tolerated dose in human body ranged from 0.545 to 0.934 mg/(kg·d). Oral rat acute toxicity ranged from 1.923 to 2.347 mol/kg, and hepatotoxicity was absent in all compounds except for QSF1. AMES toxicity was absent in both PSV1 and SCR1. Supplementary Figure S5 depicts the BOILED-Egg model for gastrointestinal absorption and blood brain barrier permeability. Out of the six ligands, PSV1 showed permeability to both the gastrointestinal tract (GI) and BBB, and situated inside the yellow region. CAT1, SCR1, CIP1, and OMB1 were in the white portion of the BOILED-Egg that indicated these four ligands were permeable to the gastrointestinal wall. In the BOILED-Egg model, QSF1 failed to be permeable to either the GI or the BBB and was situated outside the BOILED-Egg. HYP1 and CTX1 were out of the plot. CAT1 and CIP1 were positive for permeability glycoprotein (PGP), indicating that they could be easily pumped out by the permeability glycoprotein type of ATP-binding cassette transporter. Meanwhile, PSV1, OMB1, and SCR1 failed to serve as substrates of PGP (Supplementary Figure S5).

3.3 Carcinogenicity of phytochemicals

All the six phytocompounds were evaluated for carcinogenicity. According to the CarcinoPred-EL server, all compounds were classified as non-carcinogenic (Supplementary Table S4).

3.4 Toxicity class and LD_{50} value

The toxicity assessment of bioactive phytochemicals from *P. hydropiper* revealed that CAT1 was classified as toxicity class VI, whereas SCR1, QSF1, OMB1, and HYP1 were categorized as class V, and PSV1 was classified class IV. CIP1 and CTX1, as the reference antibiotics, were categorized as class IV and VI, respectively (Supplementary Table S5).

3.5 MDS of CATI-potein interactions

Based on MD, pharmacokinetics, and toxicity properties, CAT1 was simulated with two bacterial proteins (3QP1 from *C. violaceum* and *P. aeruginosa* 5BX9 protein). After simulation, RMSD values of 3QP1-CAT1 complex ranged from 0.000 5 to 0.280 0 nm with an average of 0.200 0 ± 0.020 0 nm (Figure 2A), and the value for the backbone after least square fitting was 0.150 0 nm (Figure 2B). RMSD values of 5BX9-CAT1 ranged from 0.000 5 to 0.190 0 nm with an average of 0.150 0 ± 0.009 0 nm (Figure 2C), and the value for the backbone after least square fitting was 0.10 nm (Figure 2D).

The RMSF value of protein-ligand complex (3QP1-CAT1) was 0.40 nm and the distance between heavy backbone atoms was 0.07 nm (Figure 2E and 2F). The RMSF value of ligand heavy atoms was 0.02 nm. The RMSF value of protein-ligand complex (5BX9-CAT1) was 0.10 nm and distance between heavy backbone atoms was 0.06 nm (Figure 2G and 2H). The RMSF value of ligand heavy atoms was 0.03 nm. A total of 399 hydrogen bonds in the 3QP1-CAT1 complexes were found (Figure 2I). The radius of gyration of the backbone atoms and C-alpha during the simulation were 1.57 and 1.58 nm, respectively (Figure 2J). The solvent accessible surface value of 3QP1-CAT1 complex was 105 nm^2 (Figure 2K). A total of 845 hydrogen bonds in protein complex (5BX9-CAT1) between protein and ligand were found (Figure 2L), and the radius of gyration of backbone atoms and C-alpha during the simulation were 2.24 and 2.25 nm, respectively (Figure 2M), with the solvent accessible surface value of 5BX9-CAT1 complex at 192 nm^2 (Figure 2N). The interaction energy of the protein-ligand complex (3QP1-CAT1) was determined using coulombic short-range (C-SR)/electrostatic energy and Lennard-Jones short-range (LJ-SR)/Van der Waals energy. The values for C-SR-Ligand-rest and LJ-SR-ligand-rest were – 225.76 and – 81.20 kcal/mol, respectively, while the values for C-SR-protein-ligand and LJ-SR-protein-ligand were – 30.47 and – 43.68 kJ/mol, respectively (Figure 2O). The interaction energy of the (5BX9-CAT1) complex for C-SR-ligand-rest and LJ-SR-ligand-rest was – 187.69 and – 51.15 kJ/mol, respectively, while for C-SR-protein-ligand and LJ-SR-protein-ligand, was – 41.50 and – 51.91 kJ/mol, respectively (Figure 2P). Based on the binding free energy of linear interaction obtained from 50 ns of MDS, the binding free energy of the complex of 5BX9 and CAT1 was – 84.71 kJ/mol, and the 3QP1 with CAT1 was – 95.59 kJ/mol.

3.6 Antibacterial activity of CAT1 and in combination with antibiotics

The antibacterial activity of CAT1 against six pathogenic bacteria (gram-positive and gram-negative) was represented in Figure 3A. The ZDIs were 10 – 18 mm (at 125 μg/mL), 12 – 21 mm (at 250 μg/mL), 15 – 24 mm (at 350 μg/mL), and 17 – 27 mm (at 500 μg/mL). The antibiogram of test bacteria indicates all six bacterial strains were resistant to PIP1 (6 – 14 mm), CAZ1 (6 – 9 mm), and CTX1 (6 – 12 mm) as per CLSI criteria shown in Table 4 – 6. Figure 3A and 3B showed the combined antibacterial activity of CAT1 with antibiotic ceftazidime and

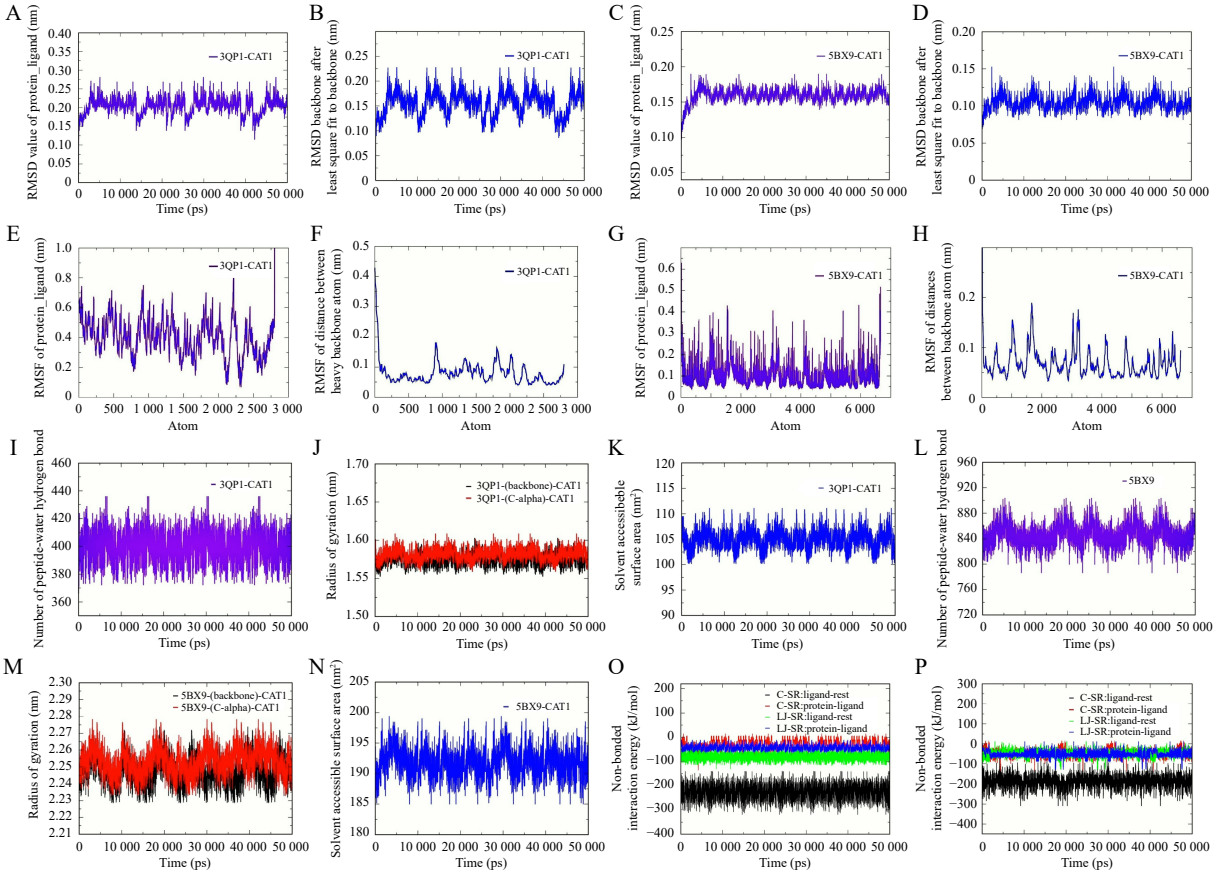

Figure 2 MDS analysis of protein-ligand complexes

A, RMSD of protein-ligand complex (3QP1-CAT1). B, RMSD of backbone after least square fitting to backbone. C, RMSD of protein-ligand complex (5BX9-CAT1). D, RMSD of backbone after least square fitting to backbone (5BX9-CAT1). E, RMSF of protein-ligand complex (3QP1-CAT1). F, RMSF of distance between heavy backbone atoms (3QP1-CAT1). G, RMSF of protein-ligand complex (5BX9-CAT1). H, RMSF of distance between heavy backbone atoms (5BX9-CAT1). I, number of peptide water-hydrogen bonds (3QP1). J, radius of gyration backbone (3QP1-CAT1) and C-alpha (3QP1-CAT1). K, solvent accessible surface area (3QP1-CAT1). L, number of peptide water-hydrogen bond (5BX9). M, radius of gyration backbone (5BX9-CAT1) and C-alpha (5BX9-CAT1). N, solvent accessible surface area (5BX9-CAT1). O, non-bonded interaction energy of CviR from *C. violaceum* (3QP1) with catechin after MDS. P, non-bonded interaction energy of *P. aeruginosa* glycoside hydrolase (PslG) (5BX9) with catechin (CAT1) after MDS.

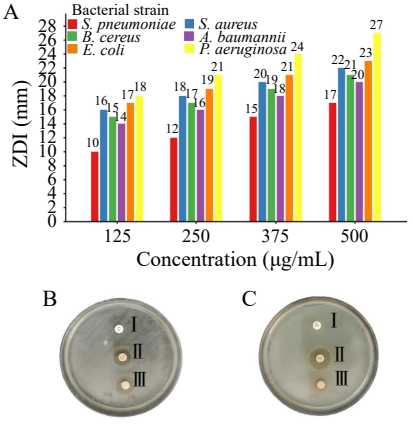

Figure 3 Antibacterial activity of CAT1 against gram-positive and gram-negative pathogenic bacterial isolates

A, antibacterial activity of three gram-positive and three gram-negative bacteria. B, combined antibacterial activity of *S. aureus*. I, ceftazidime (CAZ1) (30 μg/disc). II, CAT1 (250 μg/mL) + CAZ1 (30 μg/disc). III, CAT1 (250 μg/mL). C, combined antibacterial activity of *A. baumannii*. I, piperacillin (PIP1) (100 μg/disc). II, CAT1 (250 μg/mL) + PIP1 (100 μg/disc). III, CAT1 (250 μg/mL).

piperacillin against gram-positive *S. aureus* and gram-negative *A. baumannii*. PIP in combination with CAT1 showed synergistic effects, the GIIs ranged from 0.69 to 1.00, CAZ1 and CTX1 with CAT1 also showed similar synergistic effects, and the GIIs ranged from 0.88 to 1.00 and 0.87 to 1.00, respectively, against three gram-positive and three gram-negative bacteria (Table 4 – 6).

Table 4 The GII values from combined antibacterial activity of PIP1 and CAT1 against pathogenic bacterial isolates

Bacterial strain	ZDI (mm)			GII
	PIP1	CAT1	PIP1+ CAT1	
S. pneumoniae	14	12	18	0.69
S. aureus	6	18	24	1.00
B. cereus	9	17	25	0.96
P. aeruginosa	12	16	25	0.89
A. baumannii	8	19	23	0.85
E. coli	10	21	27	0.87

Table 5 The GII values from combined antibacterial activity of CAZ1 and CAT1 against pathogenic bacterial isolates

Bacterial strain	ZDI (mm)			GII
	CAZ1	CAT1	CAZ1 + CAT1	
S. pneumoniae	7	12	17	0.89
S. aureus	6	18	22	0.91
B. cereus	9	17	23	0.88
P. aeruginosa	9	16	22	0.88
A. baumannii	6	19	24	0.96
E. coli	6	21	27	1.00

Table 6 The GII values from combined antibacterial activity of CTX1 and CAT1 against pathogenic bacterial isolates

Bacterial strain	ZDI (mm)			GII
	CTX1	CAT1	CTX1 + CAT1	
S. pneumoniae	7	12	18	0.94
S. aureus	9	18	24	0.88
B. cereus	6	17	21	0.91
P. aeruginosa	9	16	25	1.00
A. baumannii	6	19	23	0.92
E. coli	12	21	29	0.87

4 Discussion

In this study, we examined the bioactive compounds present in *P. hydropiper* and determined the lead compounds with the highest antibacterial potential and drug-likeness properties [9]. Six bioactive compounds were selected, and their drug-likeness was evaluated based on Lipinski's RO5, ADMET analysis (including oral bioavailability, the BOILED-Egg model, and toxicity analysis), carcinogenicity, and toxicity classification [18-23]. MD was performed to assess the binding affinity of these compounds towards four bacterial target proteins. Among the six compounds, CAT1 showed the best binding performance across all the target proteins and was selected for MDS. Furthermore, to validate the antibacterial activity of CAT1, both MDS and *in vitro* studies were conducted. Natural flavonoids, as an indispensable components, were responsible for various types of biological activity, with significant pharmaceutical and medicinal value [28]. Previous studies have assessed the antibacterial activities of OMB1, SCR1, HYP1, and QSF1 [28-30]. Flavonoids inhibited bacterial nucleic acid synthesis, energy metabolism, biofilm formation, and cytoplasmic membrane function, with hydroxyl groups enhancing activity and hydrophobic substituents aiding membrane permeation [28]. SCR1 showed strong antibacterial effects against pathogens like *Streptococcus pyogenes* and *S. aureus* without cytotoxicity [30]. QSF1 inhibited SARS-CoV-2 receptors with binding energies of – 8.1 and – 8.4 kcal/mol, respectively, and demonstrated neuroprotective activity by binding to the 67-kDa laminin receptor [31]. OMB1, the α-amylase inhibitor, showed potential as an anti-diabetic drug [32]. CAT1 damaged bacterial membranes, inhibited biofilm formation in *E. coli*, and downregulated the *acrA* gene, with a docking affinity of – 8.2 kcal/mol [33].

4.1 MD analysis

Computer-aided drug design tools assist in the identification of novel inhibitor (ligand) molecules by virtue of their binding affinity for receptor molecules [34]. Various interactions between protein and ligand molecules were conducive to the inhibition mechanism [35]. The active site of a protein molecule is the region where ligand molecules bind and modulate the normal function of the protein. The specific amino acids present in the active site, can facilitate the binding of ligands within these regions [36]. Protein-ligand interactions occurred through different mechanisms, such as the lock-and-key model, induced fit, and conformational selection, which led to the disruption of the proteins' normal functions [35]. The higher binding affinity with more negative binding energy indicates greater efficacy of the ligand as a potential drug [23]. In the current study, the catalytic amino acids present within the active sites of the target proteins were identified (3FV5: aspartate, arginine, glycine, serine, and tyrosine; 3U2K: arginine and glutamic acid; 3QP1: aspartate, serine, methionine, lysine, and histidine; 5BX9: tyrosine, histidine, and glutamate) [36]. Both the docking tools showed similar results (Supplementary Table S1 and S2). The channel regions of the four proteins where ligand molecules enter and accommodate were identified [17], while the mode of binding to the active sites of the receptor proteins was also determined. Previous study has reported that indicaxanthin demonstrated inhibitory activity against IKKβ, a key target for treating inflammation and cancer-related conditions, with a comparable docking score to that of the current study [37]. Similarly, a few substituted benzimidazole and indazole compounds were docked with the human angiotensin receptor using the induced-fit approach, yielding BE ranging from – 5.036 to – 7.947 kcal/mol and identifying them as potential inhibitors [38]. Furthermore, we found various interactions, including hydrophobic and conventional hydrogen bonds that contributed to the formation of docked complexes between protein and ligand molecules. Among the compounds tested, OMB1 demonstrated the lowest binding energy of – 7.1 kcal/mol against 3FV5, with two conventional hydrogen bonds formed. The shortest bond length was observed with Glu46 at 2.39 Å. For the *S. aureus* 3U2K, OMB1 and CAT1 showed the lowest binding energies of – 8.4 and – 7.9 kcal/mol, respectively. Four conventional hydrogen bonds were formed in OMB1, while one was formed in CAT1. The shortest bond lengths

were Asp81 (2.20 Å) for OMB1 and Arg84 (2.88 Å) for CAT1. Both CAT1 and PSV1 exhibited low BE against the 3QP1 protein, responsible for quorum sensing, with binding energies of – 9.3 and – 8.9 kcal/mol, respectively. With CAT1, two conventional hydrogen bonds were formed with the shortest distance to Ser155 (2.14 Å). The 5BX9 protein showed the lowest BE of – 8.5 kcal/mol with PSV1, which formed a single conventional hydrogen bond with Gln241 (2.96 Å). Stable binding through hydrogen bonds with bond lengths < 3.5 Å was considered favorable in MD, and other types of interactions within the complex can further strengthen the binding effect [34].

Binding affinity for selected ligand molecules against target proteins is a crucial aspect of *in silico* drug discovery [39, 40]. Considering the BE values of protein-ligand complexes, we found all the ligand molecules exhibited the BE that is much superior to those of the two standard antibiotics (CIP1 and CTX1). CAT1 exhibited excellent binding energy against all the target protein molecules, suggesting that the studied phytochemicals possessed potential inhibitory effects against bacterial proteins. Previous study has reported that an isolated phyto-component from *Alstonia scholaris* was found to inhibit biofilm formation by *P. aeruginosa* through both *in vitro* and *in silico* methods [41]. Additionally, the inhibition of bacterial virulence factors, including quorum sensing and biofilm formation, has been demonstrated using phytochemicals in both *in silico* and *in vitro* analyses [42]. Quercetin showed a BE of – 10.3 kcal/mol against LAS-R protein and acted as a potent inhibitor in both *in silico* and *in vitro* studies, suggesting its capability against foodborne pathogens, which is similar to the current findings [43]. CAT1, derived from *Camellia sinensis*, has demonstrated antimicrobial activity against various microbes, including bacteria. Several synthesized CAT1 derivatives, docked in the ATP binding pocket of DNA gyrase B, showed significant antibacterial activity against different bacterial strains, which is similar to current MD results [44].

4.2 Pharmacological properties and drug-likeness analysis of bioactive compounds

Based on previous studies, compounds classified as oral drugs must meet certain physicochemical criteria [43]. Our selected ligands were evaluated for drug-likeness, and out of six, five obeyed Lipinski's RO5, apart from hyperin. The synthetic accessibility score provided insights into the synthetic complexity and knowledge crucial for drug development [44]. The bioavailability scores for CAT1, SCR1, and PSV1 were 0.55, while the values for QSF1 and HYP1 were 0.11 and 0.17, respectively. The synthetic accessibility score ranged from 1.98 to 5.32. Additionally, the BOILED-Egg plot revealed that PSV1 in the yellow region, can easily penetrate the BBB and gastrointestinal wall. CAT1, SCR1, and OMB1, in the white region, showed significant permeability to the intestinal wall. The remaining ligands showed poor permeability through either the GI or the BBB. A comparable outcome was observed in CAT1 and CIP1, both of which were PGP+, suggesting that unnecessary amounts of the drug may be pumped out through the cell membrane by PGP [21].

In drug discovery, most failures in drug development can be ascribed to the insufficient understanding of a drug's ADMET properties [45]. In our study, absorption parameters of selected phytochemicals, including intestinal absorption and the use of a human colorectal adenocarcinoma (Caco-2) cell line model, indicated good absorption rates. However, PSV1 and OMB1 had the highest log Papp values and intestinal absorption rates [43]. Within blood circulation, drug compounds can either bind to serum proteins or remain unbound, indicating the efficiency with which they may traverse cell membranes. The predicted fraction unbound values ranged from 0.087 to 0.161 fraction unbound. Furthermore, BBB and central nervous system (CNS) permeability tests indicated low distribution through the BBB, but the log PS values for PSV1 and OMB1 suggested CNS permeability. The metabolism of our selected ligand molecules was evaluated using models of cytochrome P450 isoforms. None of the ligands served as substrates for CYP2D6 and CYP3A4, except for PSV1, which was a substrate of CYP3A4. SCR1, PSV1, and OMB1 were the three inhibitors of CYP1A2, while none of the ligands inhibited CYP2C19 or CYP2C9, except for PSV1. Additionally, none of the phytochemicals served as the substrates of OCT2, which is responsible for renal deposition and clearance. The total clearance values indicated that most of the phytochemicals were easily cleared from vital organs, including the liver and kidneys, through excretion [33]. The oral acute toxicity in rats (LD_{50}) and maximum tolerated dose in humans both indicated low levels of toxicity. However, the results of CAT1, QSF1, OMB1, and HYP1 were positive in AMES test, while SCR1 and PSV1 showed negative results in AMES toxicity. Hepatotoxicity warnings were absent for all compounds except for QSF1. Overall, the ADMET properties suggested that these molecules could be easily degraded and were harmless. Based on the ADMET analysis, pharmacophore property analysis, and bioavailability score, the six selected ligands exhibited the necessary parameters required for drug molecules [43].

4.3 Analysis of carcinogenic potential of phytochemicals

The carcinogenicity test was conducted using the CarcinoPred-EL server, which utilizes three ensemble models that incorporate seven different fingerprints (CDK, CDKExt, CDKGraph, PubChem, KR, KRC, and MACCS). These fingerprints were generated for over a thousand diverse compounds, using rat carcinogenicity data from the Carcinogenic Potency Database, derived through the

PaDEL-descriptor. A probable carcinogenicity value greater than 0.5 is typically considered carcinogenic. However, in our study, all the bioactive compounds exhibited average probability values ranging from 0.27 to 0.43, indicating that they are non-carcinogenic. Moreover, the standard antibacterial drugs used in this study, CIP1 and CTX1, showed average probability values between 0.35 and 0.45, which also suggests they are non-carcinogenic. Therefore, based on these results, the bioactive compounds studied here are considered safe, with no concerns for carcinogenicity [46].

4.4 Toxicity class analysis of phytochemicals

The toxicity profiles showed that all six bioactive molecules had significant potential as drug candidates, with CAT1 performing the best across all evaluated aspects. Additionally, the LD_{50} values indicated that these bioactive phytochemicals exhibited low levels of toxicity, with further support for their potential in drug development [47].

4.5 MDS analysis of CAT1-protein complexes

This study utilized MDS to assess CAT1 inhibitory potential against two bacterial target proteins, revealing its stable binding to the active sites throughout the 50 ns simulation period [47]. The simulations provided insights into ligand-protein interactions, including RMSD, RMSF, hydrogen bonding, solvent accessible surface area (SASA), and the radius of gyration, highlighting the stability and flexibility of the protein-ligand complexes [48, 49]. CAT1 maintained low RMSF values for backbone atoms (0.07 nm for CviR and 0.06 nm for glycoside hydrolase), ligand heavy atoms (0.02 – 0.03 nm), and protein-ligand complexes (0.04 – 0.10 nm), indicating minimal fluctuations. Average RMSD values for the 3QP1-CAT1 and 5BX9-CAT1 complexes were 0.20 and 0.15 nm, respectively, confirming overall system stability. SASA values were 105 nm^2 for 3QP1-CAT1 and 192 nm^2 for 5BX9-CAT1, which are essential for evaluation of protein-ligand interactions. Hydrogen bonding was prominent, with 399 bonds in the 3QP1-CAT1 complex and 845 in the 5BX9-CAT1 complex, emphasizing strong binding [47]. Radius of gyration values (1.57 – 1.58 nm for 3QP1 and 2.24 – 2.25 nm for 5BX9) demonstrated compactness and stability post-ligand binding. These findings underscore the potential effect in CAT1 to form stable complexes with bacterial virulence-associated proteins, supported by robust molecular dynamics data [15].

CAT1, bound to 3QP1 and 5BX9, showed binding stability during MDS, as assessed through conformation property analysis using RMSD, RMSF, radius of gyration, and SASA. Linear interaction-based free energy computation and MD results showed a high correlation with each other. Previous studies have revealed that the free binding energy is crucial in structure-based computational research for identifying inhibitor molecules. A study conducted by ASHLEY et al. [49] predicted that monkeypox virus inhibitors using MM/PBSA-based binding energy calculations, with tecovirimat showed the highest binding energy of – 68.674 kJ/mol. Linear interaction energy has also been applied to estimate the energetic stability of interactions between [({(S)-1-[(1H-indol-2-yl)methyl]-3-pyrrolidinyl}methyl)amino](5-methyl-2H-pyrazol-3-yl)formaldehyde and 1-[(R)-2-(1,3-benzimidazol-2-yl)-1-pyrrolidinyl]-2-(4-methyl-1,4-diazepan-1-yl)-1-ethanone against the coronavirus main protease (3CLpro), with interaction energies of – 3.5 ± 1.7 and – 8.5 ± 1.9 kcal/mol, respectively, suggesting their potential as inhibitors [50]. In our study, both C-SR/electrostatic energy and LJ-SR/Van der Waals energy were considered for free binding energy calculation. The 5BX9-CAT1 complex exhibited a linear interaction-based free energy of – 84.71 kJ/mol, while the 3QP1-CAT1 complex presented a binding free energy of – 95.59 kJ/mol, showing the energetic stability and good inhibitory potential in these values. CAT1 showed stronger binding affinity along with less binding free energy against both the bacterial proteins, suggesting its potential as an effective inhibitor molecule.

4.6 Antibacterial activity of CAT1

CAT1, a polyphenolic compound, is known for its activity against both gram-positive and gram-negative bacteria [33]. According to a previous study, the expression of virulence factors is suppressed by the CAT1 [51]. Study has suggested that the bacteria treated with CAT1, can alter the bacterial cell structure and morphology, leading to cell separation and membrane rupture [52]. This indicates that CAT1 may facilitate effectiveness of antibiotics, and enhance bacterial zone of inhibition. In the current study, antibacterial activity was observed against both gram-positive and gram-negative bacteria. Additionally, antibiotics that were ineffective against six pathogenic bacteria showed increased ZDIs when combined with CAT1. With the growth inhibitory index, the increase in ZDI indicates a synergistic effect. Therefore, the various modes by which antibiotics, combined with CAT1, act against bacterial pathogens may help mitigate several priority pathogens as identified by the WHO. Lastly, plant-derived phytocompounds, like CAT1, have fewer side effects and greater applicability in combination with antibiotics, which can enhance antibacterial activity.

Overall, bioactive compounds from *P. hydropiper* demonstrated potential as antibacterial agents. MD revealed strong binding scores of these compounds against bacterial virulence proteins, supported by MDS and binding free energy calculations. Drug-likeness and ADMET analysis confirmed their pharmacological potential. *In vitro* experiments demonstrated CAT1 antibacterial activity against gram-positive and gram-negative bacteria. This study highlights the potential of *P. hydropiper*-derived compounds as accessible, plant-based

alternatives to antibiotics, offering efficacy against resistant bacteria with reduced side effects.

This study has certain limitations. First, the analysis of bioactive compound CAT1 conducted *in vitro* shows that it has the strongest antibacterial activity, while its direct application remains elusive. Second, the *in vitro* antibacterial activity of all the compounds was not performed. Third, clinical studies on all bioactive phytocompounds are crucial to evaluate their toxicity and determine the appropriate dosage for each compound. Despite these limitations, the current study effectively screened bioactive compounds from *P. hydropiper* with the integrated methods of *in silico* and *in vitro*, demonstrating the potential applicability of these lead molecules against bacterial infections. However, as this represented in the early stage of drug development, further clinical investigations are strongly recommended.

5 Conclusion

This study highlighted the anti-bacterial potential of *P. hydropiper* phytochemicals, including CAT1, HYP1, OMB1, PSV1, QSF1, and SCR1, against bacterial virulence proteins. These compounds demonstrated excellent binding energies and favorable pharmacokinetic properties, with MDS confirming the stability of CAT1-protein complexes involving CviR, 3QP1, and 5BX9. CAT1 exhibited notable antibacterial activity against both gram-positive and gram-negative bacteria, with enhanced effects observed when combined with antibiotics, indicating synergistic potential. These findings highlight the potential of *P. hydropiper* phytochemicals, particularly CAT1, which could serve as promising agents for combating bacterial infections. However, further clinical investigation is required to validate these findings.

Fundings

Research Grants of Senior Research Fellowship in favor of first author (Gloak Majumdar) from Council of Scientific and Industrial Research (CSIR, New Delhi, Government of India) (CSIR-SRF) with Award No. 09/1151/(0008) 2020-EMR-I.

Competing interests

The authors declare no conflict of interest.

References

[1] ASLAM B, WANG W, ARSHAD MI, et al. Antibiotic resistance: a rundown of a global crisis. Infection and Drug Resistance, 2018, 11: 1645–1658.

[2] COLLABORATORS AR. Global burden of bacterial antimicrobial resistance in 2019: a systematic analysis. Lancet, 2022, 399(10325): 629–655.

[3] World Health Organization. Antimicrobial resistance. 2025. Available from: https://www.who.int/news-room/fact-sheets/detail/antimicrobial.

[4] World Health Organization. WHO publishes list of bacteria for which new antibiotics are urgently needed. 2024. Available from: https://www.who.int/news/item/27-02-2017-who-publishes list-of-bacteria-for-which-new-antibiotics-are-urgently-needed.

[5] DE OLIVEIRA DMP, FORDE BM, KIDD TJ, et al. Antimicrobial resistance in ESKAPE pathogens. Clinical Microbiology Reviews, 2020. doi: 10.1128/CMR.00181-19.

[6] MANDAL MD, MANDAL S. Honey: its medicinal property and antibacterial activity. Asian Pacific Journal of Tropical Biomedicine, 2011, 1(2): 154–160.

[7] GHOSH C, SARKAR P, ISSA R, et al. Alternatives to conventional antibiotics in the era of antimicrobial resistance. Trends in Microbiology, 2019, 27(4): 323–338.

[8] TRINH TT, VU TA, BUI LNH, et al. Thermal and gastric stability of antimicrobial activity of juices and aqueous extracts prepared from common eligible herbs and traditional medicinal plants against *Burkholderia pseudomallei* and other enteric bacteria. Future Journal of Pharmaceutical Sciences, 2022, 8(1): 35.

[9] AYAZ M, AHMAD I, SADIQ A, et al. *Persicaria hydropiper* (L.) delarbre: a review on traditional uses, bioactive chemical constituents and pharmacological and toxicological activities. Journal of Ethnopharmacology, 2020, 251: 112516.

[10] LI H, KOMORI A, LI MD, et al. Multi-ligand molecular docking, simulation, free energy calculations and wavelet analysis of the synergistic effects between natural compounds baicalein and cubebin for the inhibition of the main protease of SARS-CoV-2. Journal of Molecular Liquids, 2023, 374: 121253.

[11] CHTITA S, BELAIDI S, QAIS FA, et al. Unsymmetrical aromatic disulfides as SARS-CoV-2 mpro inhibitors: molecular docking, molecular dynamics, and ADME scoring investigations. Journal of King Saud University-Science, 2022, 34(7): 102226.

[12] GAO Y, GUO L, HAN Y, et al. A combination of *in silico* ADMET prediction, *in vivo* toxicity evaluation, and potential mechanism exploration of brucine and brucine N-oxide-a comparative study. Molecules, 2023, 28(3): 1341.

[13] CHEN GZ, SWEM LR, SWEM DL, et al. A strategy for antagonizing quorum sensing. Molecular Cell, 2011, 42(2): 199–209.

[14] EAKIN AE, GREEN O, HALES N, et al. Pyrrolamide DNA gyrase inhibitors: fragment-based nuclear magnetic resonance screening to identify antibacterial agents. Antimicrobial Agents and Chemotherapy, 2012, 56(3): 1240–1246.

[15] MANDAL M, MANDAL S. Molecular docking and dynamics simulation of L-hyoscyamine, *Eupatorium* and alkaloid L27 as potential inhibitors against 3CLpro of SARS-CoV-2. Drug Discovery, 2021, 15(36): 231–251.

[16] MAJUMDAR G, MANDAL S. Exploring the Inhibitory role of *Persicaria hydropiper* bioactive compounds against 2KID protein associated with *Staphylococcus aureus* biofilm formation: molecular docking and pharmacological property analysis. Research Journal of Pharmacy and Technology, 2023: 3189–3194.

[17] STOURAC J, VAVRA O, KOKKONEN P, et al. Caver Web 1.0: identification of tunnels and channels in proteins and analysis of ligand transport. Nucleic Acids Research, 2019, 47(W1):

W414–W422.

[18] LIPINSKI CA. Lead- and drug-like compounds: the rule-of-five revolution. Drug Discovery Today: Technologies, 2004, 1(4): 337–341.

[19] DAINA A, MICHIELIN O, ZOETE V. SwissADME: a free web tool to evaluate pharmacokinetics, drug-likeness and medicinal chemistry friendliness of small molecules. Scientific Reports, 2017, 7: 42717.

[20] PIRES DEV, BLUNDELL TL, ASCHER DB. pkCSM: predicting small-molecule pharmacokinetic and toxicity properties using graph-based signatures. Journal of Medicinal Chemistry, 2015, 58(9): 4066–4072.

[21] DAINA A, ZOETE V. A BOILED-egg to predict gastrointestinal absorption and brain penetration of small molecules. ChemMedChem, 2016, 11(11): 1117–1121.

[22] ZHANG L, AI HX, CHEN W, et al. CarcinoPred-EL: Novel models for predicting the carcinogenicity of chemicals using molecular fingerprints and ensemble learning methods. Scientific Reports, 2017, 7(1): 2118.

[23] BANERJEE P, ECKERT AO, SCHREY AK, et al. ProTox-II: a webserver for the prediction of toxicity of chemicals. Nucleic Acids Research, 2018, 46(W1): W257–W263.

[24] LEMKUL J. From proteins to perturbed hamiltonians: a suite of tutorials for the GROMACS-2018 molecular simulation package. Living Journal of Computational Molecular Science, 2019, l(1): 5068.

[25] RIFAI EA, DIJK M V, GEERKE DP. Recent developments in linear interaction energy based binding free energy calculations. Frontiers in Molecular Biosciences, 2020, 7: 114.

[26] MANDAL S, MANDAL MD, PAL NK. Antibacterial potential of *Azadirachta indica* seed and *Bacopa Monniera* leaf extracts against multidrug resistant *Salmonella enterica* serovar Typhi isolates. Archives of Medical Science, 2007, 3(1): 14.

[27] MANDAL S, DEBMANDAL M, PAL NK, et al. Synergistic anti-*Staphylococcus aureus* activity of amoxicillin in combination with *Emblica officinalis* and Nymphae odorata extracts. Asian Pacific Journal of Tropical Medicine, 2010, 3(9): 711–714.

[28] SHAMSUDIN NF, AHMED QU, MAHMOOD S, et al. Antibacterial effects of flavonoids and their structure-activity relationship study: a comparative interpretation. Molecules, 2022, 27(4): 1149.

[29] YUAN GJ, GUAN YY, YI HQ, et al. Antibacterial activity and mechanism of plant flavonoids to gram-positive bacteria predicted from their lipophilicities. Scientific Reports, 2021, 11(1): 10471.

[30] VIOLANTE IMP, CAROLLO CA, SILVA LI, et al. Cytotoxicity and antibacterial activity of scutellarein and carajurone-enriched fraction obtained from the hydroethanolic extract of the leaves of *Fridericia chica* (Bonpl.) L.G. Lohmann. Natural Product Research, 2021, 35(23): 5287–5293.

[31] GOPALAKRISHNA R, OH A, HOU L, et al. Flavonoid quercetin and its glucuronide and sulfate conjugates bind to 67-kDa laminin receptor and prevent neuronal cell death induced by serum starvation. Biochemical and Biophysical Research Communications, 2023, 671: 116–123.

[32] KIKIOWO B, AHMAD I, ALADE AA, et al. Molecular dynamics simulation and pharmacokinetics studies of ombuin and quercetin against human pancreatic α-amylase. Journal of Biomolecular Structure & Dynamics, 2023, 41(20): 10388–10395.

[33] JUBAIR N, R M, FATIMA A, et al. Evaluation of catechin synergistic and antibacterial efficacy on biofilm formation and *acrA* gene expression of uropathogenic *E. coli* clinical isolates. Antibiotics, 2022, 11(9): 1223.

[34] HAN D, LU JR, FAN BY, et al. Lysine-specific demethylase 1 inhibitors: a comprehensive review utilizing computer-aided drug design technologies. Molecules, 2024, 29(2): 550.

[35] AZEEM M, MUSTAFA G, AHMED S, et al. Structure based screening and molecular docking with dynamic simulation of natural secondary metabolites to target RNA-dependent RNA polymerase of five different retroviruses. PLoS One, 2024, 19(8): e0307615.

[36] RIBEIRO AJM, TYZACK JD, BORKAKOTI N, et al. A global analysis of function and conservation of catalytic residues in enzymes. Journal of Biological Chemistry, 2020, 295(2): 314–324.

[37] ALLEGRA M, TUTONE M, TESORIERE L, et al. Evaluation of the IKKβ binding of indicaxanthin by induced-fit docking, binding pose metadynamics, and molecular dynamics. Frontiers in Pharmacology, 2021, 12: 701568.

[38] SILKY S, NEERUPMA D, ARUN G. Inhibitory perspective of new synthesized compounds against angiotensin receptor: Schrodinger-based induced-fit molecular docking. Journal of Pharmaceutical Research International, 2021: 79–87.

[39] MAJUMDAR G, MANDAL S. Antibacterial activity analysis of kaempferol and its derivatives targeting virulence and quorum sensing associated proteins by in silico methods. The Microbe, 2025, 6: 100259.

[40] MANDAL M, MANDAL S. Discovery of multitarget-directed small molecule inhibitors from *Andrographis paniculata* for Nipah virus disease therapy: molecular docking, molecular dynamics simulation and ADME-Tox profiling. Chemical Physics Impact, 2024, 8: 100493.

[41] ABINAYA M, GAYATHRI M. Inhibition of biofilm formation, quorum sensing activity and molecular docking study of isolated 3,5,7-trihydroxyflavone from *Alstonia scholaris* leaf against *P. aeruginosa*. Bioorganic Chemistry, 2019, 87: 291–301.

[42] KARTHICK RAJA NS, GOWRI SK, VIVEK JM, et al. *In silico* and *in vitro* analysis of quorum quenching active phytochemicals from the ethanolic extract of medicinal plants against quorum sensing mediated virulence factors of *Acinetobacter baumannii*. Indian Journal of Biochemistry & Biophysics, 2019, 56(4): 276–286.

[43] MAJUMDAR G, MANDAL S. Evaluation of broad-spectrum antibacterial efficacy of quercetin by molecular docking, molecular dynamics simulation and *in vitro* studies. Chemical Physics Impact, 2024, 8: 100501.

[44] KUMAR D, POORNIMA M, KUSHWAHA RN, et al. Antimicrobial and docking studies of (–)-catechin derivatives. Journal of the Korean Society for Applied Biological Chemistry, 2015, 58(4): 581–585.

[45] MANDAL M, MANDAL S. MM/GB(PB)SA integrated with molecular docking and ADMET approach to inhibit the fat-mass-and-obesity-associated protein using bioactive compounds derived from food plants used in traditional Chinese medicine. Pharmacological Research-Modern Chinese Medicine, 2024, 11: 100435.

[46] DIVYA RAJASELVI N, JIDA MD, NAIR DB, et al. Toxicity prediction and analysis of flavonoid apigenin as a histone

deacetylase inhibitor: an in-silico approach. In Silico Pharmacology, 2023, 11(1): 34.
[47] ARULANANDAM CD, HWANG JS, RATHINAM AJ, et al. Evaluating different web applications to assess the toxicity of plasticizers. Scientific Reports, 2022, 12(1): 19684.
[48] PIERONI M, MADEDDU F, DI MARTINO J, et al. MD-ligand-receptor: a high-performance computing tool for characterizing ligand-receptor binding interactions in molecular dynamics trajectories. International Journal of Molecular Sciences, 2023, 24(14): 11671.
[49] ASHLEY CN, BRONI E, WOOD CM, et al. Identifying potential monkeypox virus inhibitors: an *in silico* study targeting the A42R protein. Frontiers in Cellular and Infection Microbiology, 2024, 14: 1351737.
[50] JUKIČ M, JANEŽIČ D, BREN U. Ensemble docking coupled to linear interaction energy calculations for identification of coronavirus main protease (3CLpro) non-covalent small-molecule inhibitors. Molecules, 2020, 25(24): 5808.
[51] MA Y, DING SJ, FEI YQ, et al. Antimicrobial activity of anthocyanins and catechins against foodborne pathogens *Escherichia coli* and *Salmonella*. Food Control, 2019, 106: 106712.
[52] ALKUFEIDY RM, AMEER ALTUWIJRI L, ALDOSARI NS, et al. Antimicrobial and synergistic properties of green tea catechins against microbial pathogens. Journal of King Saud University-Science, 2024, 36(8): 103277.

蓼属植物化学成分通过分子对接、动力学模拟及 ADMET 分析对革兰氏阳性菌与阴性菌的多靶点抑制特性研究

Golak Majumdar, Shyamapada Mandal*

Department of Zoology, University of Gour Banga, Malda, West Bengal 732103, India

【摘要】目的 通过分子对接与实验验证，评估蓼属植物（*P. hydropiper*）中生物活性物质对细菌毒力蛋白的抗菌潜力。**方法** 研究蓼属植物中的六种生物活性化合物：儿茶素（CAT1）、金丝桃苷（HYP1）、奥布因（OMB1）、松脂素（PSV1）、槲皮素-3-硫酸酯（QSF1）及黄芩素（SCR1），通过分子对接评估其与四种细菌靶蛋白的结合亲和力和亲和位点，靶蛋白的蛋白质数据库标识符（PDB IDs）分别为：大肠杆菌拓扑异构酶 IV（PDB ID: 3FV5）、金黄色葡萄球菌旋转酶 ATP 酶结合域（PDB ID: 3U2K）、紫色色杆菌受体蛋白 CviR（PDB ID: 3QP1）及铜绿假单胞菌糖基水解酶（PDB ID: 5BX9）。对最具潜力的化合物-蛋白复合物进行 50 纳秒（ns）的分子动力学模拟。采用类药五原则评估药物相似性，并通过 SwissADME 和 pkCSM 网络服务器进行吸收、分布、代谢、排泄和毒性（ADMET）分析。通过纸片扩散法评估抗菌活性，测试单一化合物及其与常规抗生素 [头孢噻肟（CTX1，30 μg/片）、头孢他啶（CAZ1，30 μg/片）、哌拉西林（PIP1，100 μg/片）] 的联合作用。**结果** 分子对接显示所有化合物均具有强结合亲和力（－9.3～－5.9 kcal/mol），其中 CAT1 与 3QP1（－9.3 kcal/mol）及 5BX9（－8.4 kcal/mol）结合尤为显著。分子动力学模拟证实了 CAT1-蛋白复合物的稳定性，结合自由能分别为－84.71 kJ/mol（5BX9-CAT1）和－95.59 kJ/mol（3QP1-CAT1）。五种化合物（CAT1、SCR1、PSV1、OMB1、QSF1）均符合类药五原则且 ADMET 特性良好。所有化合物均无致癌性，其中 CAT1 属最低毒性类别（VI）。抗菌实验中，CAT1 对革兰氏阳性菌（肺炎链球菌、金黄色葡萄球菌及蜡样芽孢杆菌）[抑菌圈直径（ZDI）：10～22 mm] 和革兰氏阴性菌（鲍曼不动杆菌、大肠杆菌及铜绿假单胞菌）（ZDI：14～27 mm）均表现出显著活性。CAT1 与抗生素联用显示协同效应，生长抑制指数（GII）为 0.69～1.00。**结论** 蓼属植物的生物活性化合物（尤其是 CAT1）通过直接抑制细菌毒力蛋白及与常规抗生素的协同作用，展现广谱抗菌潜力，其良好的药理学特性与低毒性支持其作为抗细菌感染治疗药物的开发前景。

【关键词】蓼属植物化学成分；分子对接；分子动力学模拟；细菌致病相关蛋白；药代动力学